Quantification of Mixed Mode Loading and Bond Line Thickness on Adhesive Joint Strength Using Novel Test Specimen Geometry

B Watson[1], MJ Worswick[1], DS Cronin[1]

[1]Department of MME, University of Waterloo, 200 University Avenue West, Waterloo, Canada

bwatson@uwaterloo.ca, michael.worswick@uwaterloo.ca, duane.cronin@uwaterloo.ca

Abstract

This study quantifies the effect of mixed mode loading and bond line thickness on adhesive joint strength for automotive structural applications. This research is motivated by the need to address the complex loading that occurs during automotive crash events, as well as the variation in bond line thickness that may occur due to gap variability when joining mass-produced structural components. A newly developed specimen geometry for Mode II and Mixed Mode loading is presented, while a recently published test methodology was used to characterize the Mode I response. Three nominal bond line thicknesses (0.18, 0.30 and 0.64 mm), were investigated for a toughened structural adhesive and steel adherends. The traction-separation response, required for cohesive zone modeling (CZM) of adhesive joints, was determined for each combination of bond line thickness and mode of loading. Mode I loading resulted in higher peak traction and lower critical energy release rates compared to Mode II loading, with the Mixed Mode responses typically falling between Mode I and II, in relation to the loading angle tested. Increasing bond line thickness resulted in a reduction in initial stiffness and peak traction, as well as an increase in critical energy release rate for all modes of loading. Two existing CZM mixed mode failure criteria were assessed and demonstrated a good fit to the tested mixed mode responses, despite the limited ability of the CZM implementation to predict the end of the plateau region of the traction-separation response. The experimental approach described in this study was shown to provide repeatable results that could be directly used to fully define an adhesive CZM, ready for use in finite element modeling without the need for inverse modeling.

1   **Keywords**: mixed mode loading, adhesive joint strength, traction-separation response, bond line
2   thickness, cohesive zone modeling

3

4   **1   Introduction**

5   The use of adhesives in the design and production of automobile bodies-in-white has become more
6   prevalent in recent years as a means to address challenges in improving existing joining techniques and
7   joining multi-material structures [1]. Adoption of adhesives into vehicle structures has been supported by
8   improved finite element modeling techniques using the cohesive zone model (CZM) approach but is still
9   limited by the specialized tests and analysis techniques required to define the traction-separation
10   response, as described by da Silva and Campilho [2]. The CZM approach allows a more detailed description
11   of an adhesive interface than a typical tied constraint between adherends, without the high
12   computational costs associated with a full continuum definition of the adhesive [3]. Initial stiffness, peak
13   tractions and critical energy release rates in Mode I (tension) and Mode II (shear) are the minimum
14   requirements to define a traction-separation response in CZM formulations [4]. One common approach
15   to modeling toughened epoxy adhesives involves using a trapezoidal-shaped traction-separation response
16   [5], which has been extended to mixed-mode loading [6] (Figure 1). The Mode I and Mode II response are
17   defined independently using the initial stiffness (E_I and E_{II}), the plateau traction (σ_{IP} and σ_{IIP}), the critical
18   energy release rate (area under the traction-separation response; G_{IC} and G_{IIC}), and the ratio of the area
19   under the plastic portion of the traction-separation response to the total critical energy release rate (f_{GI}
20   and f_{GII}). These parameters are used to define three important separation values: the separation-to-
21   plateau (δ_I^0, δ_{II}^0), the separation-to-softening (δ_I^s, δ_{II}^s), and the separation-to-failure (δ_I^f, δ_{II}^f).
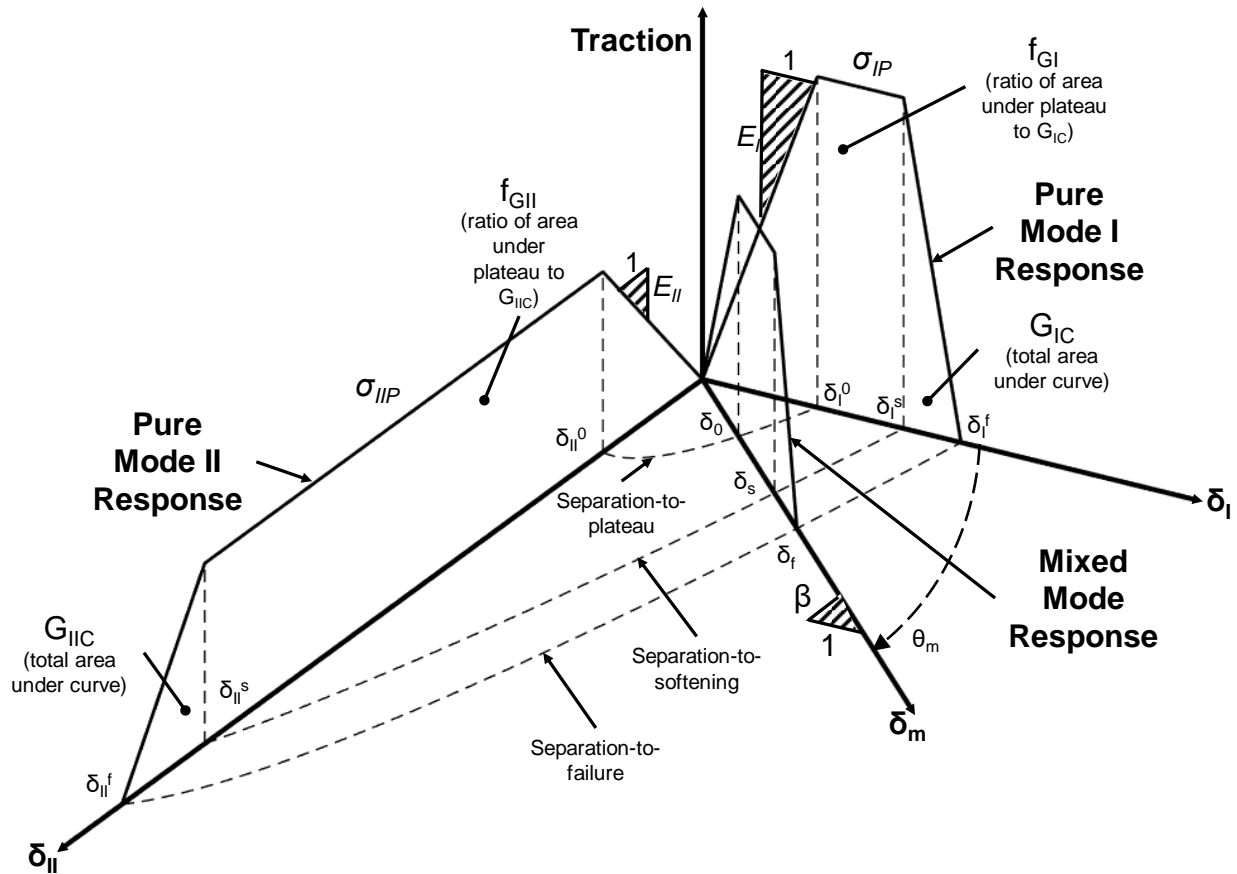
Figure 1: Mode I, Mode II and Mixed Mode response using a trapezoidal traction-separation curve [adapted from 6]

The Mode I critical energy release rate is typically measured using a double cantilever beam test [7], requiring a separate measurement for the peak traction (e.g. using a butt joint test as demonstrated by Marzi *et al.* [8]). More recently, the rigid double cantilever beam (RDCB) test, proposed by Dastjerdi *et al.* [9] for low stiffness materials, was enhanced with a new specimen geometry for testing toughened structural adhesives and an improved analysis method to enable the measurement of a complete traction-separation response from a single test [10].

The critical energy release rate in Mode II loading has been measured using the end-notched flexure test [11], while a thick adherend lap shear test [12] can be used to independently measure the Mode II peak traction. These tests can then be combined using inverse modeling to define the parameters necessary for a CZM. There are several challenges associated with end-notched flexure testing, including the commonly encountered presence of plasticity in the adherends, the assumption of pure shear (*i.e.* with

1　no compressive forces) along the neutral axis of the sample, and the need for complicated analysis

2　techniques, which often require tracking the crack front extension during testing [13]. A typical thick

3　adherend lap shear geometry, such as that described by Kadioglu *et al.* [14], is capable of providing

4　information on the pure shear (Mode II) response of the adhesive, but is not readily adapted to measure

5　the mixed-mode response of an adhesive.

6　Several authors have investigated mixed mode (MM) loading using a device that combines the double

7　cantilever beam test and end-notched flexure test, originally developed for fiber reinforced composites

8　by Benzeggagh and Kenane (BK) [15]. Liu *et al.* [16] were able to utilize this approach to measure the MM

9　loading response of a toughened structural adhesive and found that the average total energy release rate

10　was essentially the same for the Mode I and MM responses (ranging from 2.5 kN/m to 2.8 kN/m), while

11　the Mode II energy release rate was somewhat higher (3.2 kN/m). However, similar to current Mode II

12　tests, the BK mixed mode loading fixture only quantifies energy release rate while the remaining traction-

13　separation parameters must be measured using additional tests.

14　Another approach to characterize MM loading at high deformation rates was proposed by Lißner *et al.*

15　[17] who used a cylindrical specimen that was machined to provide Mode I (butt joint geometry), Mode II

16　and 45º MM loading modes, but required careful fixturing to ensure sample alignment and consistent

17　bond line thickness. Lißner *et al.* reported an increase in the critical energy release rate from Mode I to

18　Mode II loading. Conversely, the peak traction tended to decrease from Mode I to Mode II. In both cases

19　the 45º mixed mode response was between the Mode I and Mode II values.

20　To further complicate the process of characterizing adhesive joints for implementation into CZMs, the

21　parameters are dependant on bond line thickness [18]. The dependence on bond line thickness can be

22　attributed to a reduction in the constraint on the adhesive from the higher stiffness adherends as the

23　bond line thickness increases. Changing the bond line thickness alters the transition of the stress state

24　from plane stress on the specimen surface to plane strain near the center of the bond and the dimensions

25　of the fracture process zone around the crack tip. This dependency suggests that characterization of CZM

26　parameters should be carried out for the anticipated range of bond line thicknesses in a given application.

27　For example, body-in-white automotive structures have bond line thicknesses ranging from 0.2 mm to 0.5

28　mm [19], with 0.25 mm being the manufacturers recommended bond line thickness for the adhesive used

29　in this study.

1   The aim of the current study was to develop test specimen geometries and analysis techniques to

2   determine the CZM parameters required to construct complete Mode II and MM traction-separation

3   responses, building on previous research to determine Mode I parameters [10]. The effect of bond line

4   thickness on the traction-separation response for four loading angles of 0°, 45°, 75° and 90° was measured

5   and used to assess two CZM failure criteria.

6

7   **2   Summary of Mixed Mode Loading for Cohesive Zone Models**

8   When adhesive joints are subjected to loading that is not strictly in Mode I or Mode II, the mode mixity

9   (β) can be defined as [6]:

$$\beta = \frac{\delta_{II}}{\delta_I} = \tan(\theta_m) \tag{1}$$

10   Where δ_I and δ_{II} are the separations in the Mode I and Mode II directions, respectively, for a given loading

11   and θ_m (Figure 1) is the mixed mode loading angle that ranges between 0° (pure Mode I loading) and 90°

12   (pure Mode II loading). The mixed mode criterion used to define the end of the initial linear region of the

13   traction-separation response (separation-to-plateau) is often defined as [6]:

$$\left(\frac{\delta_I}{\delta_I{}^0}\right)^2 + \left(\frac{\delta_{II}}{\delta_{II}{}^0}\right)^2 = 1 \tag{2}$$

14   This relationship can be rewritten to explicitly define the mixed mode separation-to-plateau (δ^0) as a

15   function of mode mixity:

$$\delta^0 = \delta_I{}^0 \cdot \delta_{II}{}^0 \sqrt{\frac{1 + \beta^2}{\left(\delta_{II}{}^0\right)^2 + \left(\beta \delta_I{}^0\right)^2}} \tag{3}$$

16   The separation-to-softening (δ^s) can be treated similarly [6] so that:

$$\left(\frac{\delta_I}{\delta_I{}^s}\right)^2 + \left(\frac{\delta_{II}}{\delta_{II}{}^s}\right)^2 = 1 \tag{4}$$

17   Which leads to:

$$\delta^s = \delta_I{}^s \cdot \delta_{II}{}^s \sqrt{\frac{1 + \beta^2}{(\delta_{II}{}^s)^2 + (\beta \cdot \delta_I{}^s)^2}} \tag{5}$$

1   The most common MM failure criteria that have been proposed to define the separation-to-failure (δ^f)

2   when using CZMs are usually based on relationships involving energy release rates, such as the power law

3   relationship (*e.g.* Camanho *et al.* [20]):

$$\left(\frac{G_I}{G_{IC}}\right)^{\alpha} + \left(\frac{G_{II}}{G_{IIC}}\right)^{\alpha} = 1 \tag{6}$$

4   Where α is an empirical constant that must be fit to experimental data. Equation (6) can be simplified to

5   show the separation-to-failure for this criterion can be expressed as:

$$\delta^f = \frac{2(1+\beta^2)}{\delta_0}\left[\left(\frac{E_I}{G_{IC}}\right)^{\alpha} + \left(\frac{\beta^2 \cdot E_{II}}{G_{IIC}}\right)^{\alpha}\right]^{\frac{-1}{\alpha}} + \delta_0 - \delta_s \tag{7}$$

6   Another widely used MM failure criterion was proposed by Benzeggagh and Kenane [15] who were

7   attempting to experimentally quantify the Mode I and Mode II energy release rate responses with a single

8   critical energy release rate parameter for composite specimens. The authors proposed the following

9   expression (where η was fit to experimentally measured data):

$$G_I + G_{II} = G_{IC} + (G_{IIC} - G_{IC})\left(\frac{G_{II}}{G_I + G_{II}}\right)^{\eta} \tag{8}$$

10   Which leads to a separation-to-failure expression of:

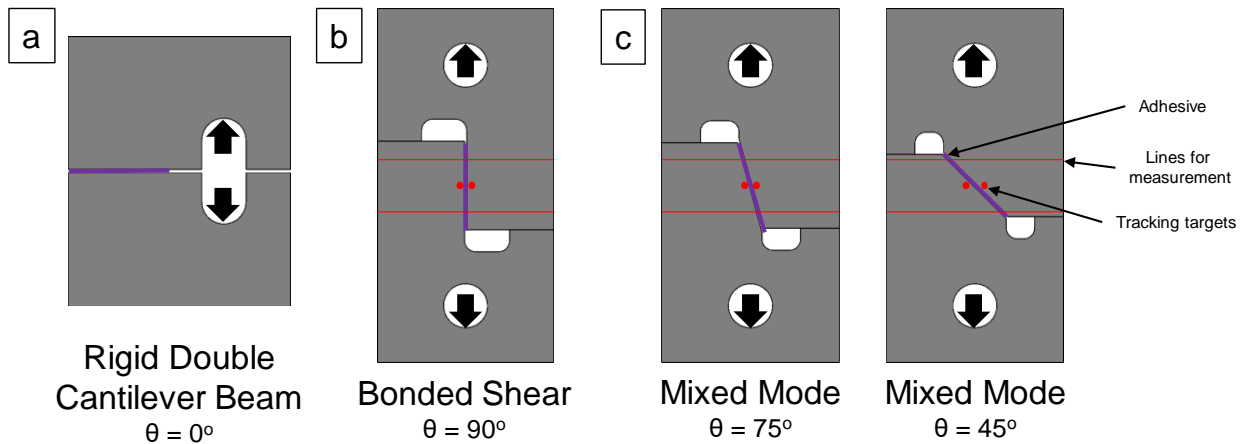$$\delta^f = \frac{2\left[G_{IC} + (G_{IIC} - G_{IC})\left(\frac{\beta^2 \cdot E_{II}}{E_I + \beta^2 \cdot E_{II}}\right)^{\eta}\right]}{\delta_0\left(\frac{E_I + \beta^2 \cdot E_{II}}{1+\beta^2}\right)} + \delta_0 - \delta_s \tag{9}$$

11

12   **3   Experimental Methodology**

13   The effect of loading mode and bond line thickness on the traction-separation response was investigated

14   using a toughened structural adhesive (3M 7333 Impact Structural Adhesive, 3M Canada Company,

15   London, Ontario Canada), building on previous characterization research with this adhesive [10]. The

16   Mode I response was measured using the RDCB specimen geometry (Figure 2a, 3a) and analysis technique

17   [10] with nominal bond line thicknesses of 0.18 mm, 0.30 mm and 0.64 mm. A new specimen geometry,

18   described as the Bonded Shear Specimen (BSS), was developed to measure the Mode II (Figure 2b) and

19   adapted to measure the MM (Figure 2c) response for the range of bond line thicknesses. The specimen

20   geometry was developed using a concept similar to a thick adherend lap shear specimen in which the

21   second moment of area was very large in the bending direction of the specimen (4336 mm^4 *vs.* 69 mm^4

1 for a typical single lap shear specimen), allowing for the assumption that all deformation was confined to

2 the adhesive. By confining all deformation to the adhesive, the complicated analysis techniques required

3 for the end-notched flexure and mixed mode beam tests, which must account for significant deformation

4 of the adherends, can be avoided in favour of a more straightforward approach. Importantly, the

5 complete traction-separation response can be extracted from a single test using the BSS and MM

6 specimens without inverse methods. In contrast, the MMB and ENF specimens provide the critical energy

7 release rate, while the peak stress must be measured from a separate test, such as the thick adherend lap

8 shear test, which often requires inverse modeling to determine all the necessary parameters. Thus, the

9 proposed methodology reduces the number of tests required to determine the CZM parameters.

10 Furthermore, the specimens in this study can be tested using simple clevises in a universal test machine,

11 while MMB testing requires specialized test fixtures. Additionally, the specimen geometry was designed

12 to enable consistent bond line thickness. Importantly, the Mode II BSS geometry was designed such that

13 the response of the adhesive could be investigated by changing the angle of the bonded surface (Figure

14 3b). In the present investigation, samples with angles of 90° (Mode II), 75° and 45° were tested in addition

15 to pure Mode I (0°) measured using the RDCB specimen. The 75° MM angle was specifically investigated

16 because it was found to correspond to the mode mixity occurring at the leading edge of a single lap shear

17 test specimen [1]. The 45° angle was the halfway point between Mode I and Mode II loading and has been

18 investigated by other authors [17]. Further reduction in loading angle was not investigated due to the

19 difficulty in measuring the small separation-to-failure as the loading angle was reduced; this issue was the

20 original motivation for the development of the RDCB specimen analysis, which relies on the somewhat

21 larger crosshead displacement rather than the smaller, noise-prone crack opening displacement used to

22 measure separation. For each mode of loading and bond line thickness tested, six repeat tests were

23 carried out.

Rigid Double
Cantilever Beam
θ = 0º

Bonded Shear
θ = 90º

Mixed Mode
θ = 75º

Mixed Mode
θ = 45º

Adhesive

Lines for
measurement

Tracking targets

Figure 2: Specimen geometries to measure Mode I (a), bonded shear (b), and mixed mode loading response (c), with bond line highlighted in red and arrows showing location and direction of loading

The samples were machined from mild steel to their respective nominal dimension (Figure 3). To assess the effect of different nominal bond line thicknesses (0.18 mm, 0.30 mm and 0.64 mm) for the BSS and MM samples, these adherends were machined with different gaps to create the desired geometry once the two adherends were bonded together.
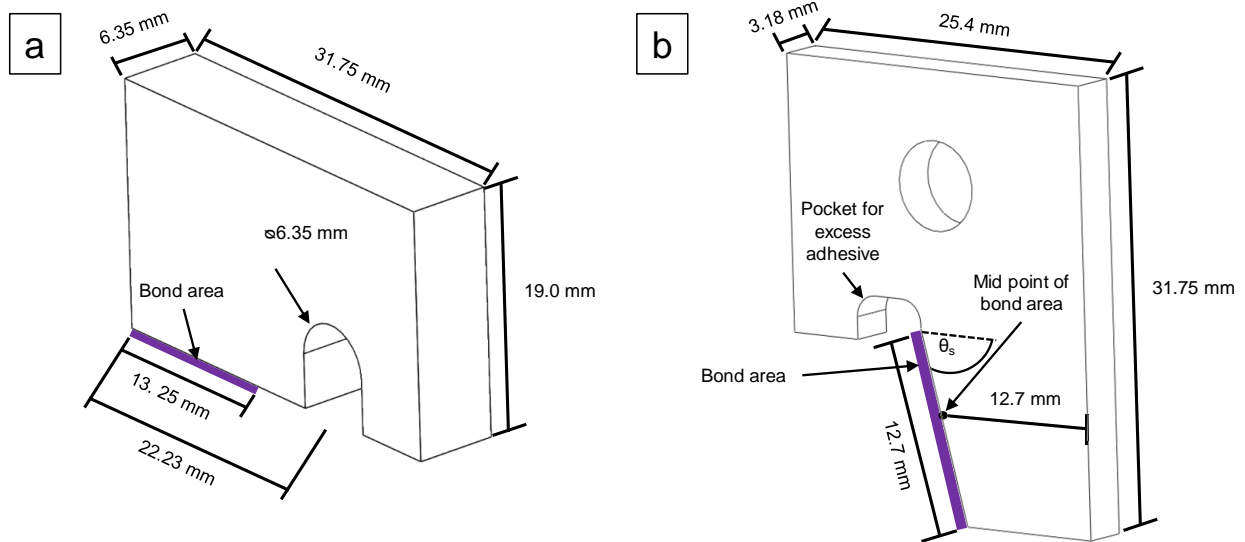
Figure 3: Dimensions of the RDCB (a), and bonded shear specimen (BSS) and mixed mode (MM) specimen adherends (b)

3.1   Test Specimen Preparation

The surfaces to be bonded were grit blasted (60 grit silicon carbide abrasive media) for roughly 10 seconds per surface at a pressure of 350 kPa and cleaned with acetone immediately prior to bonding to remove any potential contamination from the adherend surfaces.

For the RDCB specimens, a bead of adhesive was applied to the bond area of each adherend and spread to cover the entire bonded surface using a putty knife. The adherends were then located in a curing fixture with a steel shim inserted between the adherends to provide the desired bond line thickness. The edge of this shim was also used to provide a blunt notch at the leading edge of the bond line. The curing fixture was designed to ensure precise alignment of the specimens.

The BSS and MM specimens required special care to ensure a consistent bond line thickness and adherend alignment during curing. Following adhesive application to the joint surfaces, the specimens were stacked between grooved spacers in a precision ground machinists vice, which was tightened to provide enough pressure to ensure the correct bond line thickness for each specimen.

All specimens and their respective fixtures were placed in a forced convection oven (Binder ED-53; Tuttlingen, Germany) and cured for 30 minutes after reaching 80 °C, as recommended by the manufacturer. The specimen temperature was measured using a thermocouple located near the bonded location of the test specimens. After curing, the specimens were allowed to cool to room temperature in their fixtures.

All specimens had excess cured adhesive, expelled from the bond line during clamping, that was removed using a razor blade to ensure the bond area was flush to the adherend surfaces. For the BSS and MM specimens, the excess adhesive which filled the pockets at each end of the bond line (Figure 3b) was removed using a 1 mm diameter diamond coated burr. After the excess adhesive was removed from the BSS and MM specimens, two lines with a nominal spacing of 7.5 mm were marked on the surface of the specimen using an ultra fine felt tip permanent marker to provide a length gauge for optical tracking of the relative separation between the two adherends during loading. Two reference marks were also added to each of the adherends, immediately adjacent to each side of bond line, to provide tracking targets for post-test analysis. The specimens were imaged using an opto-digital microscope (ODM) (Keyence VHX 5000; Osaka, Japan) to inspect each bond line and to measure the bond line length, bond line thickness and the exact distance between the two measurement lines for each BSS and MM specimen. Specimens exhibiting any variations in bond line thickness or porosity in the bond line were not tested. Additionally,

1   for the RDCB specimens, the bond line length, distance from the specimen edge to pin loading point and

2   bond line thickness at the crack tip were measured using the ODM, as required for the test analysis

3   technique [10]. All specimen thicknesses were measured using a micrometer centered over the mid-point

4   of the bond line length.

5   **3.2   Test Procedure**

6   Testing was carried out using a hydraulic-driven load frame with a 29.7 mm (1.1675") bore x 127 mm (5")

7   stroke hydraulic cylinder (MTS Servoram 204.11; Eden Prairie, Minnesota, USA) controlled using an MTS

8   Flex Test SE hydraulic controller (MTS; Eden Prairie, Minnesota, USA). A 2.2 kN (500 lb) load cell (Omega

9   LC412-500; St. Eustache, QC, Canada) was used to measure force and a linear variable differential

10   transformer (LVDT) was used to control the displacement of the cylinder. Data was acquired at 120 Hz

11   using a National Instruments USB-6211 data acquisition system and Labview 7.1 software (National

12   Instruments; Austin, TX, USA). The tests were carried out using a constant crosshead velocity of 0.025

13   mm/s (0.001 in/s). Each test was imaged at a resolution of 1920 x 1080 pixels and 30 fps using a single,

14   digital single-lens reflex (DSLR) camera (Nikon D3200; Tokyo, Japan) fitted with a 105 mm f2.8 macro lens

15   (Sigma Corporation; Setagaya, Japan). A 2X teleconverter (Kenko TelePlus PRO 300 AF DGX 2x; Tokyo,

16   Japan) was added for RDCB testing to improve the pixel resolution of the video to approximately 95

17   pixels/mm compared to 85 pixels/mm for the BSS and MM specimens. An LED was placed in the camera

18   frame which was illuminated based on a trigger pulse from the DAC at the start of data acquisition, which

19   was then used to synchronize the test data and video.

20   **3.3   Data Analysis and Traction-Separation Fitting**

21   Image tracking (Tracker; Open Physics Project) of the reference marks on the RDCB test specimens was

22   used to determine the displacement of the loading pins. The force-displacement response of each test

23   was then used to extract the traction-separation response of the adhesive bond for each increment in the

24   force-displacement response [10]. The RDCB analysis assumes the adherends are rigid so that all of the

25   deformation occurs within the bond line, and includes consideration of the portion of the bond line that

26   is loaded in compression. The latter point is important for higher stiffness materials such as structural

27   adhesives, and was included in the proposed analysis method by Watson *et al.* [10]. Expressions for the

28   force and moment balance about the point of transition from tension to compression in the bone line

29   were derived based on the measured pin force and test specimen dimensions. The force and moment

30   balance was then solved to determine the traction and position of the transition from tension to
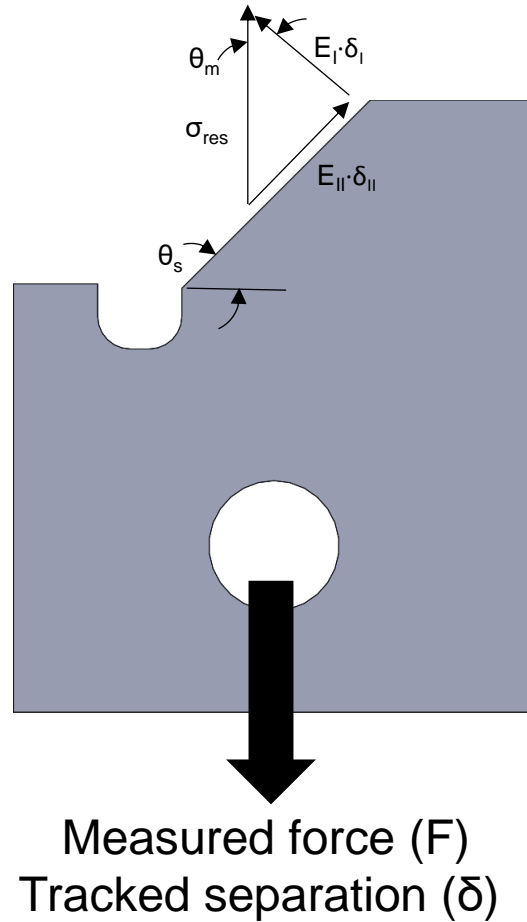
1   compression along the bond line as a function of pin displacement. By assuming the adherends to be rigid,

2   the pin displacement can be directly related to the crack opening separation and the traction-separation

3   response at the leading edge of the bond line can be calculated. The point at which the traction-separation

4   response at the crack tip reached zero traction was somewhat later than the peak force response, due to

5   the portion of the bond area near the crack tip exhibiting softening behaviour prior to the crack finally

6   opening.

7   The resultant separation (δ_m) for the BSS and MM specimens was measured by image tracking in the

8   direction of loading using the reference marks added to the adherend surfaces. For these samples, the

9   resultant traction response (σ_{Res}) was calculated by dividing the load cell force measurement by the bond

10   line length and specimen thickness measured prior to testing.

11   The RDCB and BSS measured traction-separation responses were fit to a trapezoidal response, commonly

12   used in CZM implementations for toughened structural adhesives [5]. Using a least square fit, the initial

13   stiffness (E), plateau traction (σ), critical energy release rate (G_C) and area ratio (f_G) were calculated for

14   each test. For each nominal bond line thickness, the mean value of each parameter was calculated and

15   used to generate an average traction-separation response associated with a given bond line thickness.

16   This parameter fitting was also carried out for the MM specimen tests, although for further analysis it was

17   necessary to decompose the resultant separation measurement into the Mode I and Mode II directions

18   based on the angle of mixity (θ_m, see Equation (1)) applied to the adhesive. The mixity angle was not, in

19   general, equal to the sample angle (θ_S), due to the inequality of the Mode I and Mode II initial stiffnesses

20   for a given bond line thickness. The pins used to load the samples did not support a moment, so in order

21   for a force equilibrium to exist, the direction of the resultant stress must align with the direction of loading

22   (Figure 4). Using this relationship, the mixity angle must be related to the sample angle using the following

23   expression:

$$\theta_m = \ tan^{-1}\left(\frac{E_I}{E_{II}} \cdot tan(\theta_S)\right) \tag{10}$$

Measured force (F)
Tracked separation (δ)

1

Figure 4: Schematic of the mixed mode (MM) specimen analysis

The E_I and E_{II} values used in these calculations were the mean of the values measured using the RDCB and BSS for each nominal bond line thickness. The contribution of the Mode I and Mode II energy release rates at failure were then calculated using the measured resultant separation responses and resultant plateau traction ($\sigma_{Res,P}$) by:

$$G_{I,c} = \frac{\sigma_{Res,P} \cdot cos(\theta_m)}{2}\left(\delta_I{}^f + \delta_I{}^s - \delta_I{}^0\right) \tag{11}$$

$$G_{II,c} = \frac{\sigma_{Res,P} \cdot sin(\theta_m)}{2}\left(\delta_{II}{}^f + \delta_{II}{}^s - \delta_{II}{}^0\right) \tag{12}$$

Following the procedure described above, it could be shown that for each MM test, the simple summation of $G_{I,c}$ and $G_{II,c}$ was equal to the measured critical energy release (G_c) rate by calculating the area under the MM traction (σ_{Res})-separation (δ_m) fit.

10

1 **4   Results and Discussion**

2 Force-displacement responses were measured for three bond line thicknesses under Mode I, Mode II, 75⁰

3 MM and 45⁰ MM loading. The results were fit to a trapezoidal traction-separation response and compared

4 to predictions using existing mixed-mode relationships including separation-to-plateau, separation-to-

5 softening and separation-to-failure.

6 **4.1   Rigid Double Cantilever Beam Traction-Separation**

7 The RDCB specimen Mode I response for three bond line thicknesses was used to investigate the effect of

8 bond line thickness on each parameter used to construct the Mode I traction-separation response. In all

9 cases the fracture surfaces of the RDCB samples exhibited cohesive failure. Using the force-displacement

10 response measured for each test (Figure 5a) the analysis technique described by Watson *et al.* [10] was

11 used to extract the traction-separation curve (Figure 5b). The point at which the analysis method

12 calculated zero traction at the crack tip (noted by black 'X's in Figure 5a) occurred after the peak force,

13 accounting for the plateau and softening portion of the traction-separation response. The reduction in

14 force that followed this zero-traction point can be attributed to the damage and growth of the crack in

15 the remaining bond area as continued displacement was applied.
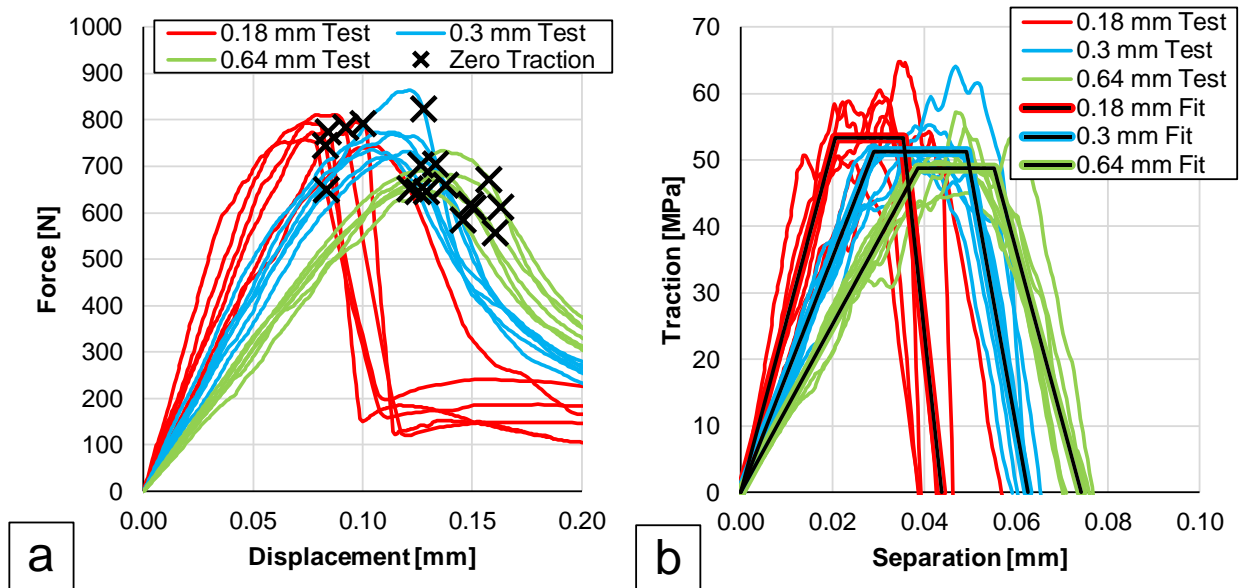
17 **Figure 5: Force-displacement (a), and traction-separation responses with average CZM fit (b)**
18 **of RDCB specimens with a nominal bond line thickness of 0.18 mm, 0.30 mm and 0.64 mm**

1   The initial stiffness (E_I), peak traction (σ_{IP}) critical energy release rate (G_{IC}) and the area ratio (f_{GI})

2   parameters extracted from each experiment were averaged to create a representative response for each

3   bond line thickness tested (Table 1). The area ratio was defined as the ratio of the area under the traction-

4   separation plateau to the total area under the complete traction-separation curve. The measured

5   separation-to-plateau, separation-to-softening, and separation-to-failure were also averaged (Table 1) for

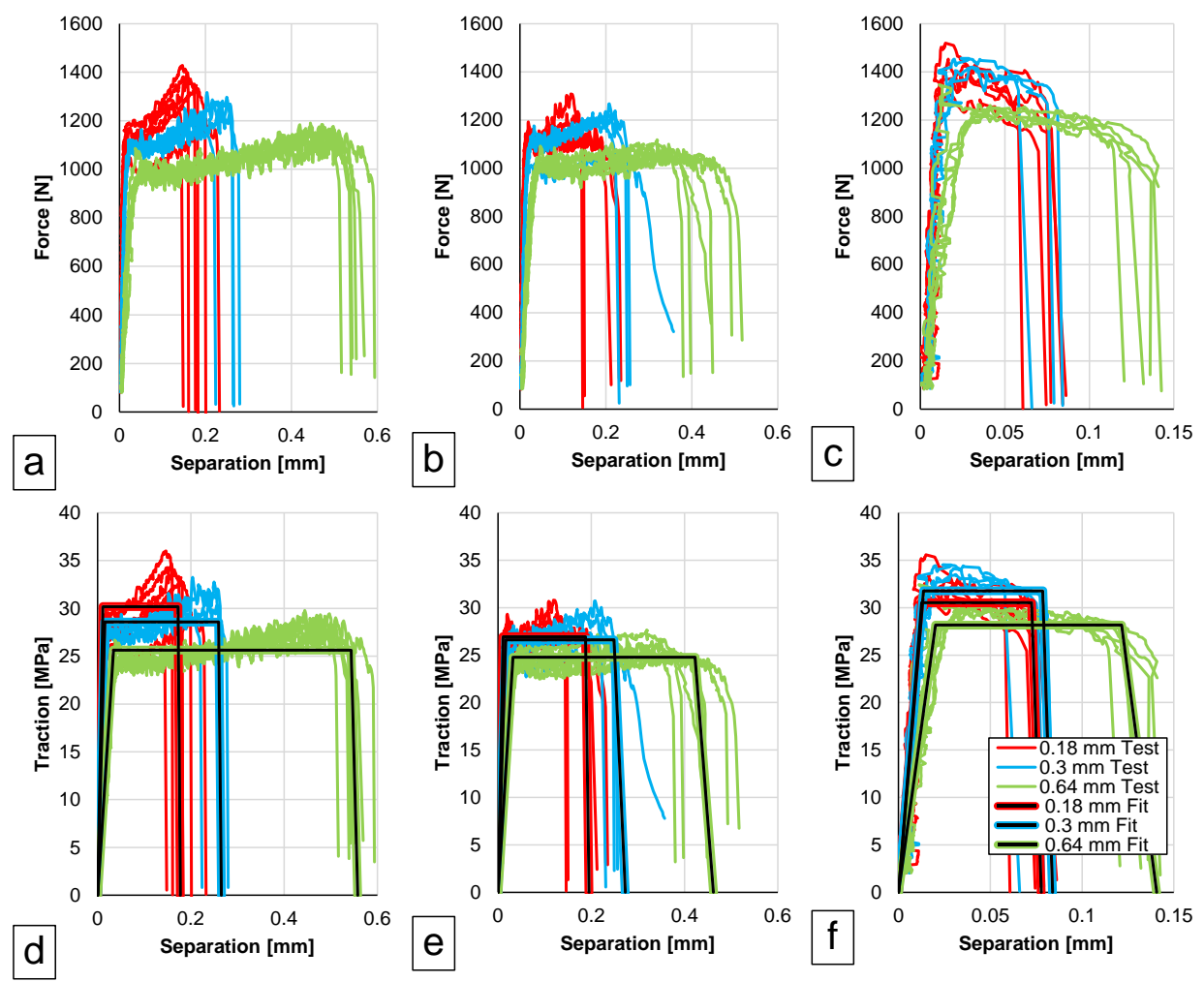6   use when assessing CZM mode mixity criteria.

7   **Table 1: Mean and standard deviation (±) of CZM parameters and separation measurements**
8   **for three nominal bond line thicknesses under Mode I loading**

Bond Line Thickness	Nominal [mm]	0.18	0.30	0.64
	Measured [mm]	0.190 ± 0.027	0.312 ± 0.005	0.626 ± 0.004
CZM Parameters	Initial Stiffness (E_I) [GPa/m]	2589 ± 629	1762 ± 203	1259 ± 118
	Peak Traction (σ_{IP}) [MPa]	53 ± 3	51 ± 5	49 ±3
	Critical Energy Release Rate (G_{IC}) [kN/m]	1.57 ± 0.21	2.13 ± 0.11	2.22 ± 0.15
	Area Ratio (f_{GI})	0.51 ± 0.05	0.49 ± 0.09	0.36 ± 0.12
Measured Separation	Plateau (δ_I^0) [mm]	0.022 ± 0.005	0.030 ± 0.006	0.039 ± 0.006
	Softening (δ_I^s) [mm]	0.037 ± 0.006	0.050 ± 0.004	0.056 ± 0.003
	Failure (δ_I^f) [mm]	0.044 ± 0.006	0.063 ± 0.002	0.074 ± 0.003

9

10   **4.2   Bonded Shear and Mixed Mode Traction-Separation Results**

11   The force-separation and traction-separation response of the BSS (Figure 6a and Figure 6d) exhibited

12   broadly similar trends to the Mode I response measured using the RDCB specimens, with decreasing initial

13   stiffness and peak traction, as well as increasing separation-to-failure, with increasing bond line thickness.

14   The measured traction-separation for each individual test was fit to a trapezoidal traction-separation

15   response. The average of the parameters (E_{II}, σ_{IIP}, G_{IIC}, f_{G2}) was calculated for each nominal bond line

16   thickness (Table 2) and was then used to define an average traction-separation response. The resultant

17   traction (σ_{Res}) and separation (δ_m) response for the $\theta_S = 75°$ (Figure 6b and Figure 6e) and $\theta_S = 45°$ (Figure

18   6c and Figure 6f) MM specimens were likewise fit to a trapezoidal traction-separation response and the

19   results were averaged to create an average traction-separation response (Table 3).

Figure 6: Force-separation, traction-separation response, and average CZM fit of 90° bonded shear (a,d), 75° mixed mode (b,e), and 45° mixed mode (c,f) specimens with a nominal bond line thickness of 0.18 mm, 0.3 mm and 0.64 mm (graphs c and f are plotted using a different scale on the x-axis for clarity)

Table 2: Mean and standard deviation (±) of CZM parameters and separation measurements for three nominal bond line thicknesses under Mode II loading

Bond Line Thickness	**Nominal [mm]**	0.18	0.30	0.64
	Measured [mm]	0.205 ± 0.026	0.382 ± 0.031	0.585 ± 0.026
CZM Parameters	**Initial Stiffness (E_{II}) [GPa/m]**	2688 ± 500	1880 ± 405	760 ± 108
	Peak Traction (σ_{IIP}) [MPa]	30 ± 2	29 ± 0.5	26 ± 0.4
	Critical Energy Release Rate (G_{IIC}) [kN/m]	5.11 ± 0.69	7.28 ± 0.66	13.69 ± 0.58
	Area Ratio (f_{GII})	0.95 ± 0.02	0.96 ± 0.01	0.96 ± 0.02
Measured Separation	**Plateau (δ_{II}^0) [mm]**	0.012 ± 0.002	0.016 ± 0.003	0.034 ± 0.004
	Softening (δ_{II}^s) [mm]	0.172 ± 0.019	0.260 ± 0.021	0.544 ± 0.019
	Failure (δ_{II}^f) [mm]	0.177 ± 0.020	0.265 ± 0.023	0.558 ± 0.031

Table 3: Mean and standard deviation (±) of CZM parameters, separation measurements and mixity angles for three nominal bond line thicknesses under mixed mode loading

		45° MM Specimen			**75° MM Specimen**		
Bond Line Thickness	**Nominal [mm]**	0.18	0.30	0.64	0.18	0.30	0.64
	Measured [mm]	0.225 ± 0.041	0.329 ± 0.036	0.603 ± 0.026	0.244 ± 0.027	0.319 ± 0.021	0.612 ± 0.019
CZM Parameters	**Initial Stiffness (E) [GPa/m]**	2416 ± 263	2333 ± 631	1395 ± 390	2538 ± 206	1616 ± 256	773 ± 90
	Peak Traction (σ) [MPa]	31 ± 1	32 ± 1	28 ± 1	27 ± 1	27 ± 1	25 ± 1
	Critical Energy Release Rate (G_C) [kN/m]	2.1 ± 0.23	2.36 ± 0.47	3.41 ± 0.39	5.01 ± 0.92	6.72 ± 0.71	10.56 ± 1.05
	Area Ratio (f_G)	0.87 ± 0.02	0.87 ± 0.06	0.84 ± 0.05	0.95 ± 0.01	0.92 ± 0.08	0.92 ± 0.07
Measured Separation	**Plateau (δ_m^0) [mm]**	0.013 ± 0.002	0.016 ± 0.005	0.023 ± 0.003	0.011 ± 0.001	0.017 ± 0.002	0.032 ± 0.004
	Softening (δ_m^s) [mm]	0.071 ± 0.007	0.084 ± 0.020	0.122 ± 0.008	0.188 ± 0.034	0.248 ± 0.012	0.424 ± 0.053
	Failure (δ_m^f) [mm]	0.077 ± 0.009	0.087 ± 0.017	0.142 ± 0.020	0.196 ± 0.041	0.277 ± 0.062	0.463 ± 0.062
Mixity Angle (θ_m) [deg]		43.9	43.9	58.9	74.5	74.0	80.8

One interesting outcome of the analysis of the MM response involved the difference between the mixity angle (θ_m) and sample angle (θ_s) for the 0.64 mm bond line thickness. The ratio of initial stiffness under

1   Mode I and Mode II loading (*i.e.* the ratio of E_I (Table 1) to E_{II} (Table 2) for a given bond line thickness) was

2   close to 1 for the 0.18 mm and 0.3 mm bond line thicknesses. For the 0.64 mm nominal bond line

3   thickness, the ratio of initial stiffness was 1.66, indicating a stronger bond line thickness dependence on

4   the initial stiffness parameter under Mode II loading compared to Mode I. Consequently, the difference

5   between the mixity angle (calculated using Equation (10)) and sample angle was much larger for the

6   thickest bond line tested.

7   The Mode II response measured in this study provided similar results to those published in the literature

8   with peak traction between 25 MPa and 31 MPa and critical energy release rates between 5.11 kN/m and

9   13.69. Lißner *et al.* [17] reported values from 30 MPa to 35 MPa and 5.0 kN/m to 12.5 kN/m, respectively,

10   for bond line thicknesses between 0.1 mm and 0. 5 mm for a rubber toughened epoxy film adhesive

11   bonding Ti-6Al-4V adherends. There was similar agreement for the 45° mixed mode case (28 MPa to 32

12   MPa and 2.10 kN/m to 3.41 kN/m in the current study *vs*. 34 MPa to 38 MPa and 2.50 kN/m to 4.60 kN/m,

13   respectively) [17]. Compared to the toughened one-part epoxy adhesive tested using the mixed-mode

14   bending apparatus by Lui *et al*. [16], the current study reported a critical energy release rate under mixed

15   mode loading that was slightly lower (2.1 kN/m *vs*. 2.8 kN/m) and a Mode II response that was somewhat

16   larger (5.11 kN/m *vs.* 3.2 kN/m) for bond line thicknesses below 0.26 mm. Direct comparisons to CZM

17   parameters presented in the literature are not possible due to differences in the adhesive formulations

18   tested. The general agreement between the values measured in the current study and other studies

19   focusing on toughened epoxy adhesive suggests that the current methodology provides reasonable

20   responses for the range of conditions tested.

21   The Mode II traction-separation response exhibited a small positive slope (Figure 6a) rather than a flat

22   plateau as assumed in the current CZM approaches, similar to the measurements made on the bulk

23   material response of the same adhesive [21]. Bulk shear testing of the adhesive used in this study,

24   described by Watson *et al.* [21], demonstrated a tangent modulus, which was roughly 1.7% of the shear

25   modulus. Comparing the slope of the plateau to the initial stiffness of all BSS tested in the current study

26   produced a mean value of 1.2 ± 0.5%. While this is a fairly crude comparison, it lends credence to the

27   notion that this rising plateau is, at least in part, related to the bulk material response, though obviously

28   the confinement effects complicate this relationship. This positive slope meant that when the CZM

29   parameters were fit to the test data, the fit response tended to overpredict the test traction for lower

30   separation values and underpredict the test traction at higher separation values of the plateau section.

1   This discrepancy was also present to some degree in the response of the $\theta_S = 75^{\circ}$ specimen response, but

2   was not apparent in the $\theta_S = 45^{\circ}$ response, which exhibited a flat plateau.

3   The BSS fracture surfaces tended to exhibit mixed cohesive-interfacial failure, with shear cusp formation,

4   such as that described by Purslow [22]. The MM specimens demonstrated a mix of fully cohesive failure

5   in Mode I and shear cusp formation in Mode II, with more cohesive failure apparent on the $\theta_S = 45^{\circ}$ MM

6   specimens, indicating a gradual progression between the two failure surface morphologies. In general,

7   the failure surface transitioned from cohesive failure in the RDCB (0°) test specimen, to mixed cohesive

8   and interfacial failure with the amount of interfacial failure increasing with the load angle. Similarly, the

9   formation of shear cusps increased from the MM samples to the BSS (90°) test specimen. This progression

10   in failure surface morphology suggests a relatively smooth transition in traction-separation response can

11   be expected between the Mode I and Mode II responses, despite differing failure morphologies.

12   One critical observation with the BSS and MM specimens was the tendency for these specimens to fail

13   much more abruptly compared to the RDCB specimens, often across only one or two camera frames. This

14   abrupt failure was primarily due to the entire bond line length being subjected to the input separation,

15   rather than the progressive loading occurring with the RDCB samples. While Lißner *et al.* [17] used

16   secondary ultra-high-speed photography to track the softening portion of the traction-separation

17   response, even for quasi-static testing, this was deemed unnecessary in the current study, which used a

18   displacement-controlled load frame to load the specimens. Lißner *et al.* measured area ratios that were

19   somewhat smaller in Mode II (0.7 to 0.5) than the current study (0.95 to 0.96) under quasi-static loading,

20   although the softening plateau behaviour in their study was not observed in the current study, making

21   direct comparison difficult.

22   While the current characterization methodology focuses on the effect of bond line thickness within the

23   bond, the use of high stiffness adherends that exhibited no appreciable deformation precludes comment

24   on the potential effects caused by the state of deformation of the adherends, often called external

25   constraint [23]. An earlier study using the RDCB methodology [10] demonstrated the ability to use CZM

26   parameters measured with the RDCB specimen to predict the experimental force-displacement response

27   of a typical tapered double cantilever beam test with a high degree of accuracy.

28   **4.3   Bond Line Thickness Effects**

29   It was apparent from the force-displacement response of the RDCB tests that, as bond line thickness

30   increased, the initial slope of the response decreased due to an increase in the joint compliance with

1 increasing bond line thickness. There was also a slight reduction in average peak force as bond line

2 thickness increased (780 ± 23 N, 766 ± 48 N, and 680 ± 27 N for 0.18 mm, 0.6 mm and 0.64 mm bond line

3 thicknesses, respectively). These effects can be attributed to the reduction in the confinement effect

4 exerted by the adherends on the adhesive as the bond line thickness increased [7]. The average Mode I

5 traction-separation response demonstrated a reduction in slope and plateau traction with increasing bond

6 line thickness, following the measured force-displacement response (Figure 7). The critical energy release

7 rate increased with increasing bond line thickness owing to the increase in separation-to-failure that

8 overwhelmed the decrease in peak traction. Using a t-test, statistically significant differences (assuming

9 α = 0.05) were identified for the initial stiffness, plateau traction, critical energy release rate and area ratio

10 (p-values of 9. 14 x 10^{-4}, 3.47 x 10^{-2}, 2.10 x 10^{-4}, 3.05 x 10^{-2}, respectively assuming a two-tailed distribution

11 and equal variance) when comparing the 0.18 mm bond line thickness results (n = 6) and the 0.64 mm

12 results (n = 6). The measured bond line thickness varied from the nominal or target bond line thickness

13 by a maximum of 0.05 mm (e.g. Figure 7), due to variability in manufacturing the test specimens.

14
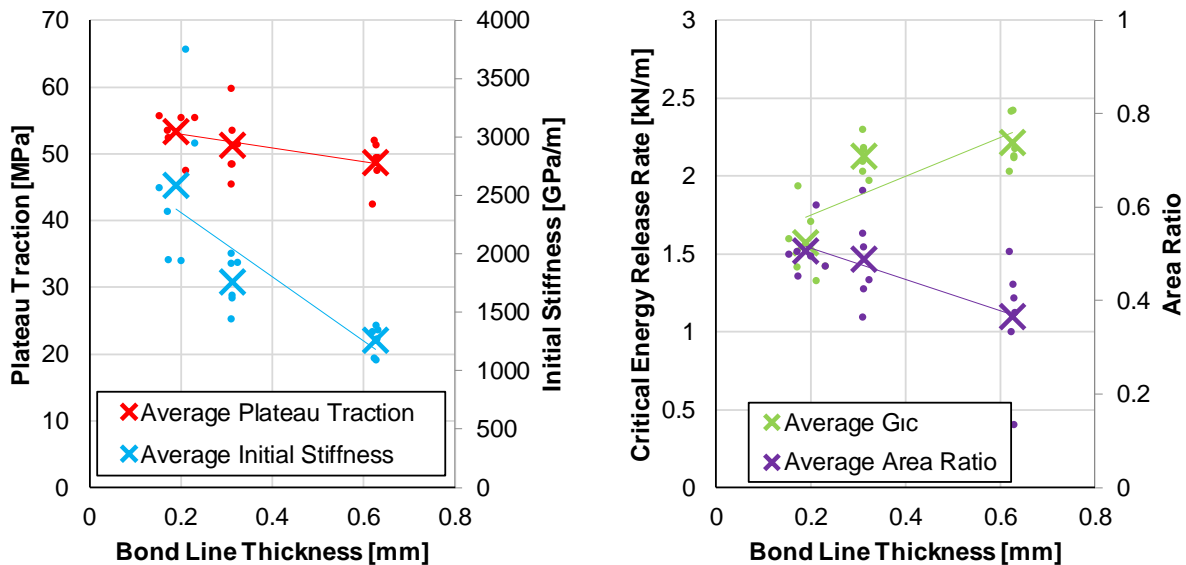
Figure 7: Mode I CZM parameters *vs.* bond line thickness measured from RDCB testing

16 The Mode II response exhibited similar trends to the Mode I response (Figure 8). This finding is in

17 agreement with the reported end-notched flexure test carried out by Boutar *et al.* [24], who found that,

18 for the range of bond line thicknesses studied in the current study, critical energy release rate correlated

19 positively with bond line thickness. T-tests were used to compare the initial stiffness, peak traction, critical

20 energy release rate and area ratio for the smallest (0.18 mm (n = 5)) to the largest (0.64 mm (n = 6)) bond

1 line thickness tested. Statistically significant differences were measured for the initial stiffness, plateau

2 traction and critical energy release rates (p-values of 1.62 x 10^{-5}, 1.62 x 10^{-4}, 8.14 x 10^{-9}, respectively) while

3 no statistical difference was apparent for the area ratio (p-value of 0.774).
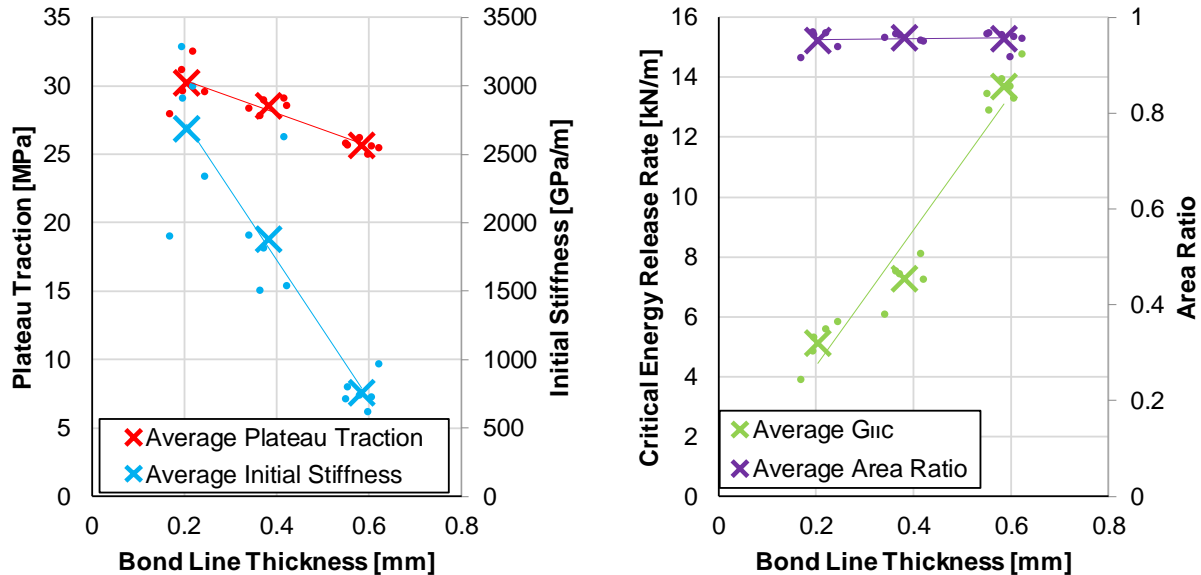
4

5 **Figure 8: Mode II CZM parameters *vs.* bond line thickness measured from BSS testing**

6 While a clear trend of increasing critical energy release rate with increasing bond line thickness was

7 present with the MM specimens, the reduction of initial stiffness and plateau traction with increasing

8 bond line thickness was less clear. These unclear trends can primarily be related to the higher standard

9 deviation in the bond line thickness for the MM specimens compared to the BSS. The MM specimens

10 required pressure in both the lateral and longitudinal directions during the curing process in order to

11 maintain a consistent bond line thickness that led to some variability, which was especially apparent with

12 the 0.18 mm nominal thickness specimens. When considering only the 0.3 mm and 0.64 mm specimens,

13 the trends seen in Mode I and Mode II are readily apparent.

14 **4.4   Mixed Mode CZM Criteria Compared to Experimental Test Results**

15 Based on the measured responses, it was possible to compare the MM response of the adhesive for all

16 modes of loading, using two existing CZM criteria.

17 The Mode I *vs.* Mode II separation-to-plateau (Figure 9a) and separation-to-softening (Figure 9b) test

18 responses were plotted, along with the CZM mixity criteria as described by May *et al*. [6] using Equation

19 (2) and Equation (4). To assess the separation-to-failure response, each test was first decomposed into

Mode I and Mode II energy release rate terms using Equation (11) and Equation (12). After decomposing the response, the power law (Equation (6)) and BK (Equation (8)) failure criteria were fit to the experimental data (Figure 9b) using a least squares method to determine the mixity parameters (α=0.83 and η=4.68) based on minimizing the error between the measured mixed-mode displacement and the fit for both mixity angles measured for each bond line thickness (*i.e.* 6 values total). This approach to the parameter fitting assumed that the mixity parameter was not a function of bond line thickness. A comparison of the Mode I and Mode II separation response (Figure 9c) was then carried out using Equation (7) and Equation (9). In these plots, the average measured response is denoted by an 'X' with the range of measured responses denoted by the colored lines for each bond line thickness while the fit response was plotted using solid greyscale lines.
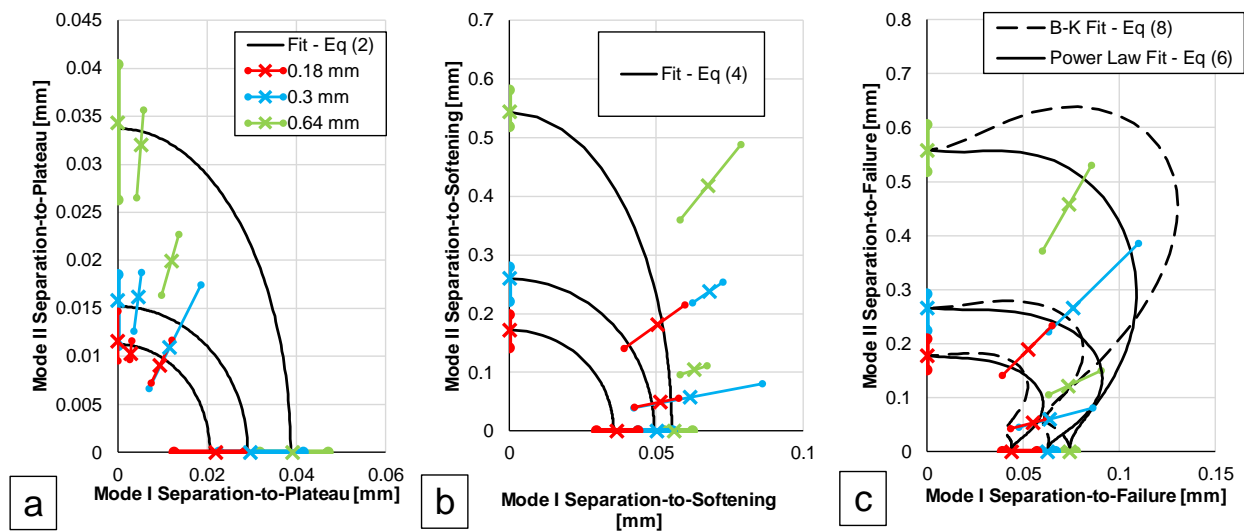
Figure 9: Mode I *vs.* Mode II separation-to-plateau (a), separation-to-softening (b) and separation-to-failure (c)

The fit of the separation-to-plateau mixity criterion (Equation (2)) fell within the measured responses, aside from the thickest bond line when loaded at θ_S = 45°, in part due to the relatively large scatter in the test data and very small separation required to reach the plateau traction. Unlike the separation-to-plateau response, the separation-to-softening response criterion (Equation (4)) underpredicted the MM response across all bond line thicknesses measured, aside from the 0.3 mm thickness at θ_S = 45°, which exhibited a large range of measured response. The power law fit of separation-to-failure predicted the θ_S = 75° test responses well (0.069 mm average difference for three bond line thicknesses), while slightly under predicting the measured response of the θ_S = 45° specimens with 0.18 mm and 0.3 mm bond line thicknesses. The fit of the BK failure criterion fell within the experimental responses with the exception of

1 the 0.64 mm, θ$_S$ = 75° specimen, which was overpredicted by the MM failure criterion. A comparison of

2 the Mode I and Mode II energy release rates at fracture (Figure 10) demonstrated that the mixity

3 parameters used to fit the experimental data (α=0.83 and η=4.68) fell within the experimental results.

4 Two exceptions were the power law fits for the 0.64 mm thick 45° overpredicting the test result, and the

5 0.3 mm thick 75° slightly underpredicting the test result.
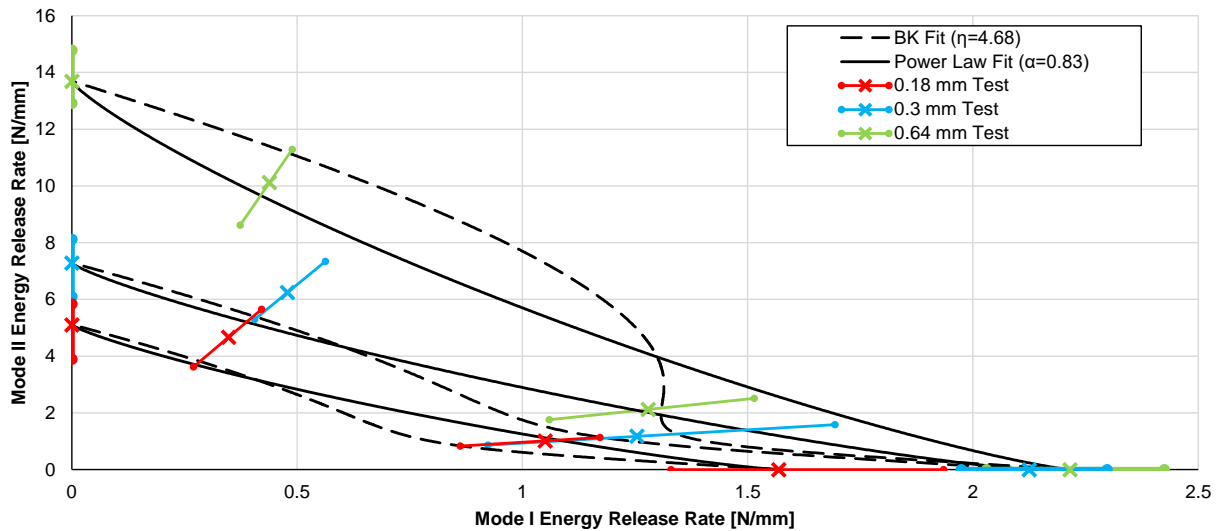
6

7 **Figure 10: Mode I *vs.* Mode II energy release rate**

8 The BK and power law failure criteria described the test response reasonably well despite using the

9 relatively ill-fitting separation-to-softening response that underpredicted the test response by as much as

10 37%. This outcome implies that, using the current criteria, the predicted traction-separation response for

11 all MM loading would have a significantly shorter plateau region and begin to soften much sooner than in

12 the measured response, potentially providing a conservative estimate of a joint strength under MM

13 loading conditions. This shortened plateau can be seen when comparing the experimental average fit to

14 the predicted response in the 0.64 mm thick, θ$_S$ = 75° case (Figure 11). The discrepancy between measured

15 and fit separation-to-softening has not been commented on previously, due to the need to use several

16 tests to measure the peak traction and critical energy release rate independently [12] and then compile

17 the results along with inverse modeling to develop a complete set of CZM parameters.
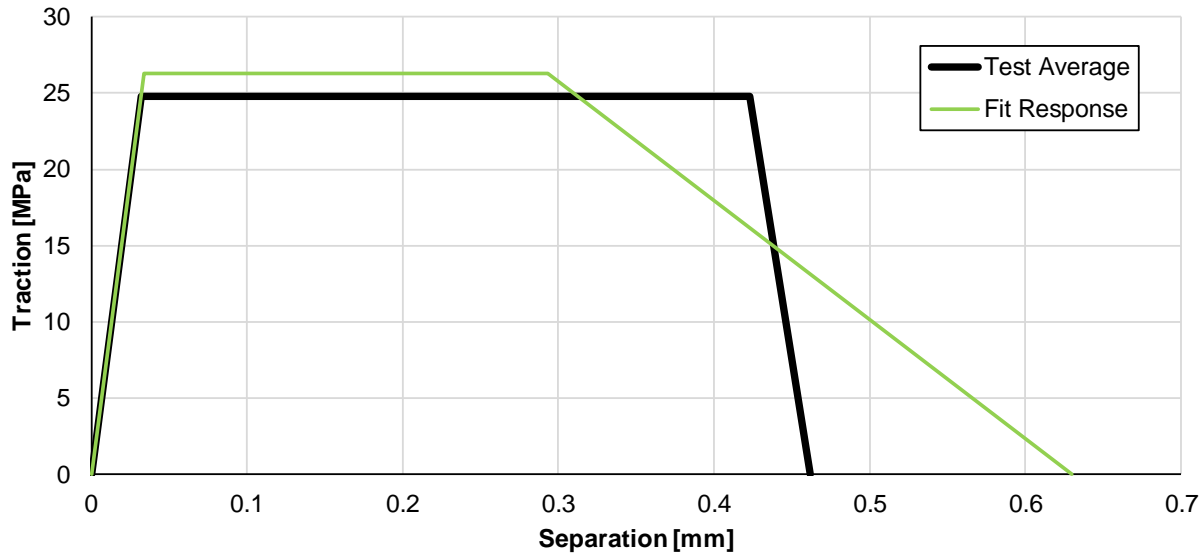
Figure 11: Comparison of test average *vs.* fit traction separation response for a bond line thickness of 0.64 mm and a sample angle of 75º

5   Conclusions

The specimen designed to measure the Mixed Mode (MM) response of bonded joints, provided measured parameters that generally fell between the Mode I (RDCB) and Mode II (BSS) responses, regardless of the bond line thickness tested. The effect of bond line thickness under Mode I and Mode II loading was characterized by a statistically significant decrease in the initial stiffness and peak traction parameters, and a statistically significant increase in the critical energy release rate. The ratio of area under the traction plateau to critical energy release rate (f_I, f_{II}) was also found to have a statistically significant increase with increasing bond line thickness in Mode I, but was found to be constant under in Mode II loading. Bond line thickness effects for the MM specimens were somewhat confounded by variability in the actual specimen bond line thickness.

While the displacement-based power law separation-to-plateau (δ^0) MM criterion was found to fit the measured response reasonably well, the separation-to-softening (δ^s) response was generally not well-predicted. Two common separation-to-failure (δ^f) criteria (the critical energy release rate-based power law [4] and the Benzeggagh-Kenane criterion [15]) were found to fit the experimental data well. However, the need to use the displacement-based separation-to-softening response to calculate separation-to-

failure suggests that further investigation is required to develop a series of criteria that fit the measured traction-separation responses for all loading modes.

The test methodology outlined in the current study has proven suitable to characterize the response of a bonded joint under Mode I through Mode II loading, along with any arbitrary MM angle. Moreover, the results of this testing have been shown to be readily adaptable for use in CZM applications.

References

1. Watson, B., Nandwani, Y., Worswick, M. J., & Cronin, D. S. (2019). Metallic multi-material adhesive joint testing and modeling for vehicle lightweighting. *International Journal of Adhesion and Adhesives*, 95, 102421. https://doi.org/10.1016/j.ijadhadh.2019.102421

2. Da Silva, L. F., & Campilho, R. D. (2012). Determination of the Cohesive Parameters. In Advances in numerical modeling of adhesive joints (pp. 28-30). SpringerBriefs in *Applied Sciences and Technology*. Springer, Berlin, Heidelberg. https://doi.org/10.1007/978-3-642-23608-2_1

3. Trimiño, L. F., & Cronin, D. S. (2016). Evaluation of numerical methods to model structural adhesive response and failure in tension and shear loading. *Journal of Dynamic Behavior of Materials*, 2(1), 122-137. https://doi.org/10.1007/s40870-016-0045-7

4. Campilho, R. D., Banea, M. D., Neto, J. A. B. P., & da Silva, L. F. (2013). Modelling adhesive joints with cohesive zone models: effect of the cohesive law shape of the adhesive layer. *International Journal of Adhesion and Adhesives*, 44, 48-56. https://doi.org/10.1016/j.ijadhadh.2013.02.006

5. Tvergaard, V., & Hutchinson, J. W. (1992). The relation between crack growth resistance and fracture process parameters in elastic-plastic solids. *Journal of the Mechanics and Physics of Solids*, 40(6), 1377-1397. https://doi.org/10.1016/0022-5096(92)90020-3

6. May, M., Voß, H., & Hiermaier, S. (2014). Predictive modeling of damage and failure in adhesively bonded metallic joints using cohesive interface elements. *International Journal of Adhesion and Adhesives*, 49, 7-17. https://doi.org/10.1016/j.ijadhadh.2013.12.001

7. Kinloch, A. J., & Shaw, S. J. (1981). The fracture resistance of a toughened epoxy adhesive. *The Journal of Adhesion*, 12(1), 59-77. https://doi.org/10.1080/00218468108071189

8. Marzi, S., Hesebeck, O., Brede, M., & Kleiner, F. (2009). A rate-dependent cohesive zone model for adhesively bonded joints loaded in mode I. *Journal of Adhesion Science and Technology*, 23(6), 881-898. https://doi.org/10.1163/156856109X411238

9. Dastjerdi, A. K., Pagano, M., Kaartinen, M. T., McKee, M. D., & Barthelat, F. (2012). Cohesive behavior of soft biological adhesives: experiments and modeling. *Acta Biomaterialia*, 8(9), 3349-3359. https://doi.org/10.1016/j.actbio.2012.05.005

10. Watson, B., Liao, C. H., Worswick, M. J., & Cronin, D. S. (2020). Mode I traction-separation measured using rigid double cantilever beam applied to structural adhesive. *The Journal of Adhesion*, 96(8), 717-737. https://doi.org/10.1080/00218464.2018.1502666

11. Chai, H. (1988). Shear fracture. *International journal of fracture*, 37(2), 137-159. https://doi.org/10.1007/BF00041716

12. May, M., Hesebeck, O., Marzi, S., Böhme, W., Lienhard, J., Kilchert, S., & Hiermaier, S. (2015). Rate dependent behavior of crash-optimized adhesives–Experimental characterization, model development, and simulation. *Engineering Fracture Mechanics*, 133, 112-137. http://dx.doi.org/10.1016/j.engfracmech.2014.11.006

13. Marzi, S., Hesebeck, O., Brede, M., & Kleiner, F. (2009b). An end-loaded shear joint (ELSJ) specimen to measure the critical energy release rate in mode II of tough, structural adhesive joints. Journal of adhesion science and technology, 23(15), 1883-1891. https://doi.org/10.1163/016942409X12508517390716

14. Kadioglu, F., Vaughn, L. F., Guild, F. J., & Adams, R. D. (2002). Use of the thick adherend shear test for shear stress-strain measurements of stiff and flexible adhesives. *The Journal of adhesion*, 78(5), 355-381. https://doi.org/10.1080/00218460211818

15. Benzeggagh, M. L., & Kenane, M. (1996). Measurement of mixed-mode delamination fracture toughness of unidirectional glass/epoxy composites with mixed-mode bending apparatus. *Composites science and technology*, 56(4), 439-449. https://doi.org/10.1016/0266-3538(96)00005-X

16. Liu, Z., Gibson, R. F., & Newaz, G. M. (2002). The use of a modified mixed mode bending test for characterization of mixed-mode fracture behavior of adhesively bonded metal joints. *The Journal of Adhesion*, 78(3), 223-244. https://doi.org/10.1080/00218460210408

17. Lißner, M., Alabort, E., Cui, H., Rito, R., Blackman, B. R. K., & Petrinic, N. (2019). Experimental characterisation and numerical modelling of the influence of bondline thickness, loading rate, and deformation mode on the response of ductile adhesive interfaces. *Journal of the Mechanics and Physics of Solids*, 130, 349-369. https://doi.org/10.1016/j.jmps.2019.06.011

18. Reedy Jr, E. D., & Guess, T. R. (1993). Comparison of butt tensile strength data with interface corner stress intensity factor prediction. *International Journal of Solids and Structures*, 30(21), 2929-2936. https://doi.org/10.1016/0020-7683(93)90204-K

19. Droste, A. (2006). Crash stable adhesives in application and simulation. In *Proc. 5th German LS-DYNA Forum*. Available on-line: https://www.dynamore.de/de/download/papers/forum06/ verbindungstechnik/crash-stable-adhesives-in-application-and. Accessed December 1, 2019.

20. Camanho, P. P., Davila, C. G., & De Moura, M. F. (2003). Numerical simulation of mixed-mode progressive delamination in composite materials. *Journal of composite materials*, 37(16), 1415-1438. https://doi.org/10.1177/0021998303034505

21. Watson, B., Worswick, M. J., & Cronin, D. S. (2019). Identification of Shear Sample Test Geometry for Bulk Adhesive Characterization. In *Mechanics of Biological Systems & Micro-and Nanomechanics, Volume 4* (pp. 47-50). Springer, Cham. https://doi.org/10.1007/978-3-319-95062-4_11

22. Purslow, D. (1986). Matrix fractography of fibre-reinforced epoxy composites. *Composites*, 17(4), 289-303. https://doi.org/10.1016/0010-4361(86)90746-9

23. Pardoen, T., Ferracin, T., Landis, C. M., & Delannay, F. (2005). Constraint effects in adhesive joint fracture. *Journal of the Mechanics and Physics of Solids*, 53(9), 1951-1983. https://doi.org/10.1016/j.jmps.2005.04.009

24. Boutar, Y., Naïmi, S., Mezlini, S., da Silva, L. F., & Ali, M. B. S. (2017). Characterization of aluminium one-component polyurethane adhesive joints as a function of bond thickness for the automotive industry: Fracture analysis and behavior. *Engineering Fracture Mechanics*, 177, 45-60. https://doi.org/10.1016/j.engfracmech.2017.03.044